Electrochimica Acta 475 (2024) 143640

Contents lists available at ScienceDirect

Electrochimica Acta

journal homepage: www.journals.elsevier.com/electrochimica-acta

Effects of N-functional groups on the electron transfer kinetics of VO^{2+}/VO_2^+ at carbon: Decoupling morphology from chemical effects using model systems

Maida A. Costa de Oliveira [a], Christian Schröder [a], Marc Brunet Cabré [a], Hugo Nolan [a,b], Antoni Forner-Cuenca [c], Tatiana S. Perova [d], Kim McKelvey [a,e], Paula E. Colavita [a,b,*]

[a] School of Chemistry, Trinity College Dublin, Dublin 2, Ireland
[b] CRANN and AMBER Research Centres, Trinity College Dublin, Dublin 2, Ireland
[c] Department of Chemical Engineering and Chemistry, Eindhoven University of Technology, 5600MB Eindhoven, the Netherlands
[d] School of Engineering, Trinity College Dublin, College Green, Dublin 2, Ireland
[e] MacDiarmid Institute for Advanced Materials and Nanotechnology, School of Chemical and Physical Sciences, Victoria University of Wellington, Wellington 6012, New Zealand

ARTICLE INFO

All authors contributed to reviewing and editing the manuscript.

Keywords:
Carbon
Vanadium
Vanadyl
Pervanadyl
Aryldiazonium
Heterogeneous charge transfer
Finite element simulations
Electrocatalysis

ABSTRACT

Carbons and nanocarbons are important electrode materials for vanadium redox flow battery applications, however, the kinetics of vanadium species are often sluggish at these surfaces, thus prompting interest in functionalization strategies to improve performance. Herein, we investigate the effect of N-functionalities on the VO^{2+}/VO_2^+ redox process at carbon electrodes. We fabricate thin film carbon disk electrodes that are metal-free, possess well-defined geometry and display smooth topography, while featuring different N-site distribution, thus enabling a mechanistic investigation of the intrinsic surface activity towards VO^{2+}/VO_2^+. Voltammetry and electrochemical impedance spectroscopy show that N-functionalities improve performance, with pyridinic/pyrrolic-N imparting the most significant improvements in charge transfer rates and reversibility, compared to graphitic-N. This was further supported by voltammetry studies on nitrogen-free electrodes modified via aryldiazonium chemistry with molecular pyridyl adlayers. Computational modeling using an electrochemical-chemical mechanism indicates that introduction of surface pyridinic/pyrrolic-N can increase the heterogeneous rate constants by approximately two orders of magnitude relative to those observed at nitrogen-free carbon ($k^0 = 1.29 \times 10^{-4}$ vs 9.34×10^{-7} cm/s). Simulations also suggest that these N-functionalities play a role in affecting reaction rates in the chemical step. Our results indicate that nitrogen incorporation via basic functional groups offers an interesting route to the design of advanced carbon electrodes for VRFB devices.

1. Introduction

Vanadium redox flow batteries (VRFBs) are an attractive technology for applications in energy storage. Since VRFB was proposed by Skyllas-Kazacos and co-workers in 1983, the progress of this technology has been widely recognized [1–3] as well as its numerous advantages such as large energy capacity, long life cycle, deep discharge capabilities, flexible capacity, and low environmental impact [1,4–6]. A VRFB is composed of two electrolyte tanks with vanadium redox couples, separated by an ion-exchange membrane; the electrolyte is circulated through a cell with porous/high surface area electrodes at which charge and discharge reactions involving V(III)/(II) and V(IV)/(V) redox processes take place. Nevertheless, control of kinetic barriers to vanadium redox switching and an understanding of the reaction mechanisms at the electrode/electrolyte interface are important for designing high-performing VRFB devices.

Carbons in, for example felt, paper and cloth forms, are among the preferred electrode materials for VRFB due to their low cost, high surface area, high conductivity, good mechanical and electrochemical stability [5,7–13]. However, the kinetics of vanadium species are often sluggish at these electrodes thus limiting overall performance; this has led to significant work in the literature aimed at optimizing carbon electrode properties to reduce resistances to charge transfer for both the V(III)/(II) and V(IV)/(V) couples. Surface modifications and

* Corresponding author at: School of Chemistry, Trinity College Dublin, Dublin 2, Ireland.
E-mail address: colavitp@tcd.ie (P.E. Colavita).

https://doi.org/10.1016/j.electacta.2023.143640
Received 28 August 2023; Received in revised form 27 October 2023; Accepted 3 December 2023
Available online 5 December 2023

pre-treatments, involving particularly oxidation and reactive heat-treatments [10,11,14–17] have been extensively explored as a route to improving performance. Promising results have also been obtained by modifying the carbon structure with other heteroatom functionalities including N, B, P and S groups [18–26]. Among these, N-doping is especially attractive due to its versatility and potential for introducing a range of functional sites to modulate activation barriers, while often also leading to enhanced carbon conductivity [24,27–31]. Nevertheless, the current understanding of the effects and the mechanism by which N-doping alters the electrochemical response of carbons towards vanadium species is limited [19,27].

Key properties such as carbon hydrophilicity, degree of graphitization and electrochemically active surface area (ECSA) have been identified to impact cell performance [10,15,32]. The presence of heteroatom functional groups is also widely acknowledged to affect the charge transfer kinetics [11,14–16,32–35] however, the exact role played by such groups in leading to observed changes is often difficult to interpret. This is because studies on porous carbon electrodes with complex morphologies and high porosity, make it challenging to untangle the impact of a specific chemical functionality on the intrinsic surface activity of the functional carbon, from the significant changes in ECSA that typically result from surface treatments required for such modifications. This problem has been eloquently highlighted in recent work by several groups [15,32,36,37]. In particular, the interpretation of changes in rate constant and faradic current densities for vanadium redox processes resulting from functionalization is not straightforward at porous electrodes. Changes in wettability/accessibility can affect the effective viscosity in the intrafilm volume, leading to dispersion in the effective diffusion coefficient of redox species, in addition to changing the electrolyte contact area [36].

To investigate the intrinsic activity of carbon materials and nanomaterials in V(III)/(II) and V(IV)/(V) reactions several groups have therefore adopted methodologies aimed at overcoming the above challenges. Tichter et al. have reported methods to accurately account for porosity and mass transport effects in carbon networks in the modeling of the electrochemical response [38,39]. Kroner et al. [40] carried out voltammetry on single carbon fiber microelectrodes extracted from felts to correctly account for electrode area in rate constant determinations. Goulet et al. [41] designed a flow-through microfluidic cell for the study of V(III)/(II) and V(IV)/(V) at porous carbons using transport-corrected Tafel analysis. Stimming and co-workers [32,36] have also discussed strategies for accounting for ECSA in rate constant determinations. Notably, Selva Kumar and Compton [37] recently demonstrated single entity nano-catalysis studies of the V(IV)/(V) reaction at carbon nanotubes to determine their intrinsic surface activity and the mechanism of reaction. The above strategies have contributed to improved understanding of the role of carbon nanostructure, degree of graphitization and the effect of hydroxyl/carbonyl groups on charge transfer kinetics [32,34,36]. However, the effect of N-functionalities on the carbon response is significantly less explored and understood, despite the promising results reported for porous N-doped carbon architectures.

In this work, we investigate the role of N-functionalities on the VO^{2+}/VO_2^+ redox process at carbon electrodes. To this end we fabricated thin film carbon materials in the form of disk electrodes that are metal-free and posses well-defined geometry and smooth topography. Using a combination of physical deposition methods and post-deposition thermal treatments demonstrated in previous work from our group [42,43], we are able to control N-content and type/distribution of nitrogen functionalities displayed at the carbon surface. The disk electrode geometry allowed for an investigation of the role of N-sites on the intrinsic surface activity of carbon electrodes towards the vanadyl oxidation in the absence of confounding effects from morphology or metal impurities. The use of topographically smooth electrodes has been previously applied by our group and others for elucidating the role of nitrogen functionalities in the electrocatalysis of the oxygen reduction reaction (ORR) [43–47], however to the best of our knowledge it has no precedent in studies of vanadyl oxidation. Our results demonstrate that N-functionalities enhance intrinsic surface activity, with basic pyrrolic/pyridinic N-sites resulting in greater improvements in charge transfer rates compared to graphitic-N. Using surface modification reactions, we show that molecular pyridyl moieties can also deliver improvements in charge transfer rates further supporting our findings. Finally, we discuss the potential role of basic N-sites with support from digital simulations and in the context of reactions proposed for vanadyl oxidation in the literature [37,48].

2. Experimental

Materials. Vanadyl sulfate hydrate (99.999 %), sulfuric acid (99.99 %), 3-aminopyridine (99.99 %), hydrochloric acid (37 %), sodium nitrite (99 %), methanol (HPCL 99.9 %) were purchased from Sigma Aldrich and used as received. Alumina slurries (1, 0.3 and 0.05 μm particle size) and polishing cloths (Micro Polishing Cloth and Nylon Polishing Ploth) were purchased from Ted Pella and Buehler, respectively. Glassy carbon disks with 5 mm o.d. (GC, Sigradur HTW) and Si wafers (300 nm thermal oxide) were used as substrate materials. A 2.00 in. diameter and 0.125 in. thick graphite target (Kurt J. Lesker, 99,999 %) was used at the sputtering source.

Fabrication of carbon thin film electrodes:. GC disks and clean Si were used as substrates for the fabrication of carbon thin films depending on the requirements of specific characterization methods. GC disks were polished to a mirror finish as previously reported [28], with alumina slurries, with disks being cleaned for 10 min in Millipore water between steps to avoid cross contamination. Carbon thin film electrodes were fabricated via a combination of physical deposition and post-deposition treatments, as recently described [42] and as schematically shown in Fig. 1A. Briefly, carbon thin films were first deposited in a DC-magnetron sputtering chamber (Torr International, Inc.) at base pressure $< 2 \times 10^{-6}$ mbar and at deposition pressure in the range of 1–2 $\times 10^{-2}$ mbar. A graphite target was the carbon source in a 50 sccm total flow of either pure Ar or 2 % N_2/Ar (by flow), yielding amorphous carbon (a-C) and nitrogenated amorphous carbon (a-C:N) thin films, respectively. Carbon thin films were subsequently annealed at 900 °C following conditions described in [42]: a-C and a-C:N were annealed under N_2 flow for 1 h, yielding films referred to as anC and anC:N_G, respectively; a-C was also annealed under NH_3/N_2 yielding film electrodes referred to as anC:N_P. For a summary of experimental conditions see **Table S1**.

Carbon functionalization:. Functionalization reactions were carried out using 3-aminopyridine as a precursor for diazotization reactions to form the corresponding aryldiazonium cation [49] as schematically shown in Fig. 1**B**. A 5 mM solution of 3-aminopyridine was prepared in 0.625 M HCl containing 2 % CH_3OH. The solution was cooled in an ice bath for 1 h, then a 50 mM $NaNO_2$ solution was added to it dropwise yielding a final concentration of nitrite of 10 mM. After complete diazotization all functionalization experiments were carried out using the 4.0 mM solution of the diazonium cation thus prepared. Electrochemically driven functionalization was carried out by using the carbon substrate as the working electrode in a 3-electrode cell and applying −0.45 V vs Ag/AgCl for 10 s, yielding samples referred to as anC-EPy; cyclic voltammetry was used to confirm that the potential of −0.45 V results in electroreduction of the diazonium cation as in [49]. After functionalization all samples were washed in Millipore water and CH_3OH and dried under N_2 flow.

Characterization:. X-ray Photoelectron spectroscopy (XPS) was performed using an Omicron ESCA system with a monochromatic Al K X-ray source (1486.7 eV). Carbon samples were prepared on Si wafer substrates; survey and high resolution scans were obtained at 50 and 15 eV pass energy, respectively. Spectra were fitted using commercial software (CasaXPS) using a Shirley background and Voigt peak functions. Atomic compositions were determined from peak area ratios, after correction for relative sensitivity factors (RSF: C1s = 1.0, N1s = 1.8 and

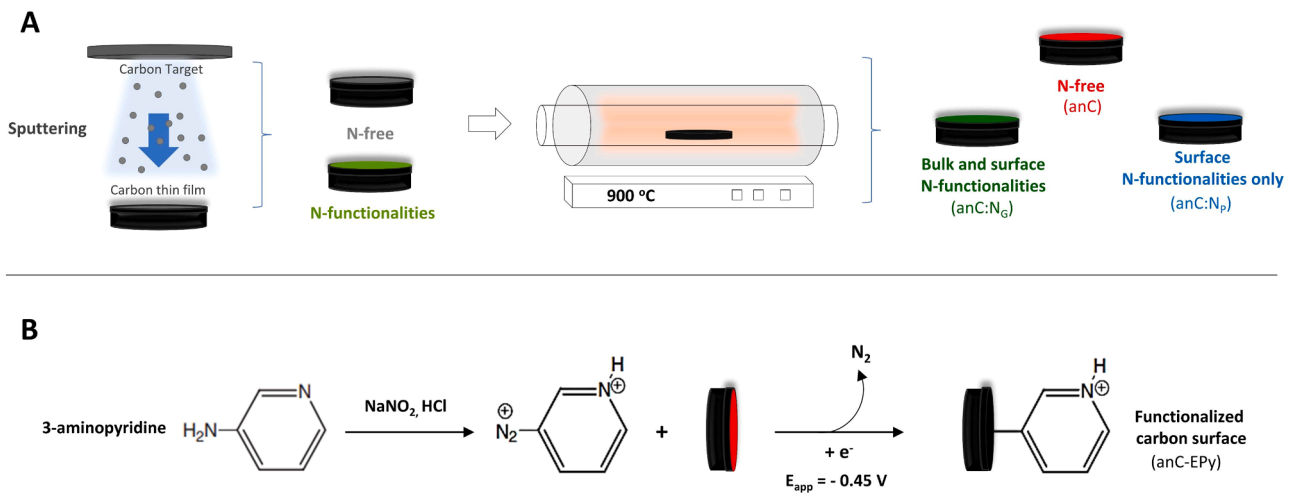

Fig. 1. (A) Main steps in the fabrication of thin film carbon electrodes via sputtering deposition and post-deposition thermal treatments. (B) In situ diazotization reaction and electrochemical functionalization of carbon disk electrodes using 3-aminopyridine precursors.

O1s = 2.93). Atomic force microscopy was carried in a Park system NX10 with 350 GHz Si tips in non-contact mode. Raman spectra were measured in backscattering configuration using a Renishaw 1000 micro-Raman system with He-Ne laser excitation at 633 nm. Static water contact angles were measured using a goniometer (FTA1000).

Electrochemistry:. Electrochemical measurements were carried out on a potentiostat (Metrohm Autolab) using static and rotating electrode (Pine Instruments) methods. A 3-electrode cell was used with a graphite rod as counter electrode (CE), Ag/AgCl as reference electrode (RE) and the GC disks as working electrode (WE). The cell was filled with 100 mL of electrolyte, as indicated in each case, and thermostated at 20 °C. Prior to all measurements, the electrolyte was purged 20 min with Ar. Cyclic voltammograms were obtained at different scan rates (0.010–0.050 V s^{-1}), as stated in each case; voltammograms obtained at 1600 rpm rotation were obtained at 0.0001 V s^{-1}. Electrochemical impedance spectroscopy (EIS) studies were performed at 1600 rpm; results were analysed using commercial software (ZView). Tafel slopes were calculated from the current logarithm plots according to the relation $\eta = a + b\log j$, where $\eta = E - E_{eq}$ is the overpotential and b is the slope value. The transfer coefficient was estimated based on $a = \frac{RT\ \ln 10}{bnF}$ [50] where R and F are the universal gas constant and Faraday's constant, respectively, temperature T = 293.15 K and number of electrons n = 1 for vanadyl oxidation. Results reported after normalization by the electrode geometric area were calculated using a mean disk area of 0.196 cm^2 previously determined by Randles Sevcik analysis with outer sphere redox couples. Digital simulations of voltammograms were carried out using finite element methods (COMSOL Multiphysics v5.3a) and further details are provided in Supporting Information.

3. Results

3.1. Preparation of N-modified carbon thin films and electrochemical studies

To investigate the effect of heteroatom groups on the electrochemical response of the VO^{2+}/VO_2^+redox couple at carbon electrode surfaces, we carried out the synthesis of thin film carbon electrodes with well-defined chemical functionalities and smooth topography. Work from our group [42] recently demonstrated that magnetron sputtering deposition followed by thermal annealing under N_2 or NH_3/N_2 atmosphere (see Fig. 1**A**) can be used to deposit smooth graphitized carbon thin film electrodes that are metal-free and display the atomic composition summarized in Table 1. Three types of carbon were prepared for our studies: anC which contained no nitrogen functionalities (see Supporting Information); anC:N_G with both bulk and surface N-functionalities of which 60 % consisted of graphitic-N (N_G) (Fig. 2**B**); and anC:N_P with N-functionalities at the surface, exclusively, that consisted of predominantly pyridinic-N (N_P) and pyrrolic-N (N_{Pyrr}) (Fig. 2**A**). All carbons displayed similarly graphitized networks, as indicated by%-area of the trigonally bonded carbon component (C_{sp^2}/C_{tot}) relative to the overall C1s carbon peak, which was found to be 68–71 % across all three materials (**Table S2**). Water contact angles were similar for anC and anC:N_G surfaces, whereas the value was lower for anC:N_P, as expected from the presence of hydrophilic pyrrolic/pyridinic N-functionalities. Finally, all carbon films were of thickness ca. 65 nm and their intrinsic roughness was low, as confirmed by R_q <1.5 nm measured on samples deposited on Si wafers (see **Fig. S2**).

Table 1
Composition (atomic-%), thickness and root-mean-square roughness (R_q) of carbon thin film electrodes used for electrochemical studies. Details of the characterization of anC:N_G and anC:N_P can be found in [42], while anC results are shown in Figs. S1–S2 and Table S2.

Carbon electrode	Components (at. %)			N 1s (at.%)			AFM morphology	
	C	N	O	N_G	N_{Pyrr}	N_P	Thickness (nm)	R_q (nm)
anC	96	–	4.0	–	–	–	65 ± 1	1.3
anC:N_G	91	3.0	6.0	60	6.0	34	65 ± 1	1.3
anC:N_P	94	0.8	5.2	16	31	53	65 ± 1	1.4

The electrochemical response of nitrogenated and N-free carbon thin film electrodes was investigated in 15 mM $VOSO_4$ in 1.5 M H_2SO_4. Fig. 2**C** shows cyclic voltammograms (CV) obtained at 20 mV s^{-1} for anC:N_P electrodes in the absence and presence of VO^{2+} in solution (both in dashed lines). The CV obtained in supporting electrolyte alone was used to subtract the capacitive background yielding the corrected CV shown with a continuous line, which displays well-defined faradaic peaks associated with the VO^{2+}/VO_2^+ redox response (E° = 0.991–1.000 V) [48,51]. The cathodic limit of 0.2 V vs Ag/AgCl ensures that VO^{2+}/V^{+3} reductions (E° = 0.38 V) [48] do not contribute significantly to the cathodic response observed.

The correction for the capacitive background contributions was carried out in the same manner for anC and anC:N_G (**Fig. S3A-3D**) and Fig. 2**D** shows a comparison of the corrected CV curves obtained at 20 mV s^{-1} at anC, anC:N_G and anC:N_P disk electrodes. Results indicate that the response is irreversible in the case of nitrogen-free anC materials, while minimal reversibility is observed at anC:N_G surfaces. For anC, the

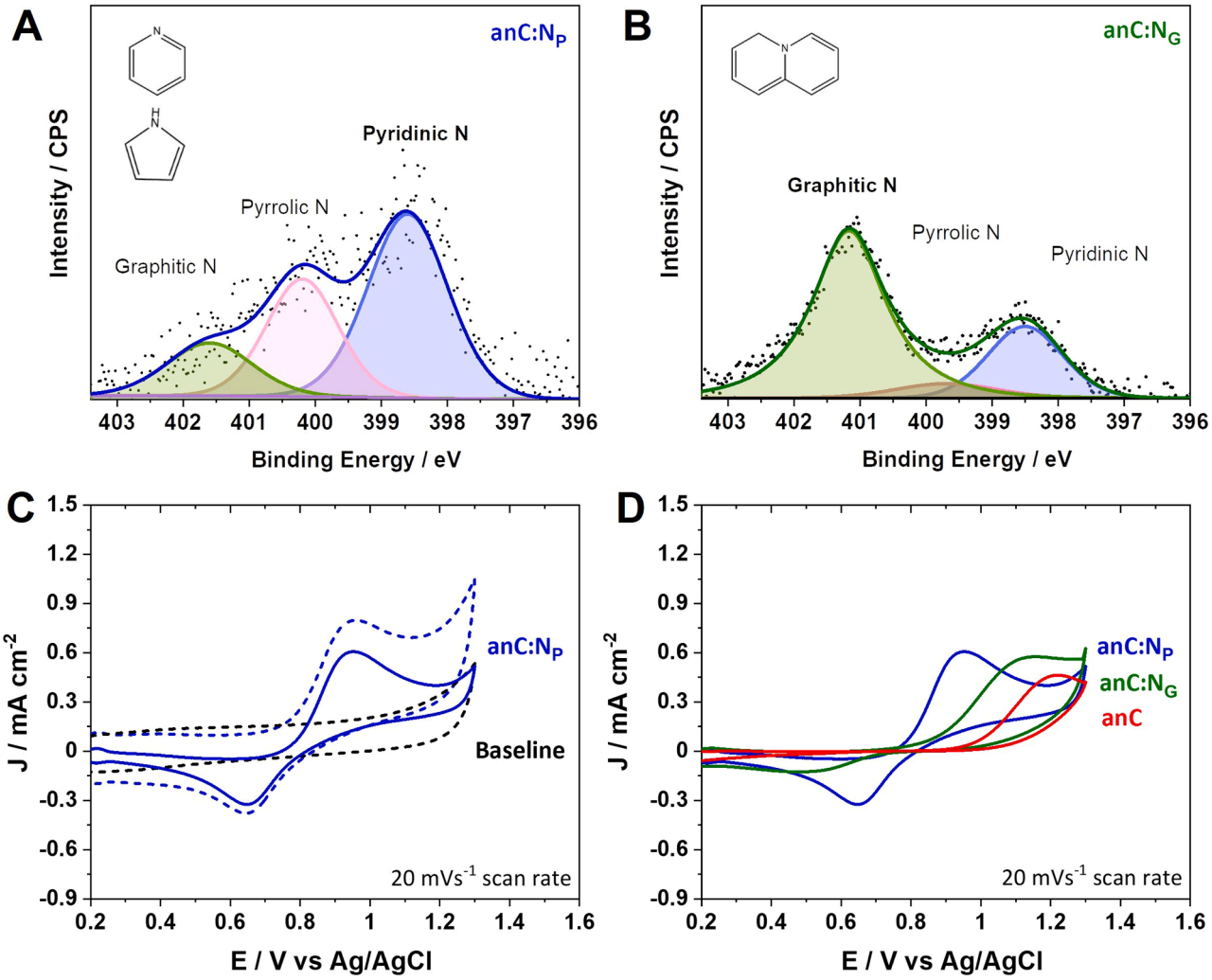

Fig. 2. High resolution N 1s XPS spectra and best fit of N-functionalities at (A) anC:NP and (B) anC:NG surfaces, as reported in previous work [42]. (C) CV at anC:NP electrodes obtained at 20 mV s−1 in 1.5 M H2SO4 (dashed black), after addition of 0.015 M $VOSO_4$ (dashed blue) and following subtraction of the capacitive background to evidence faradaic peaks (solid blue). (D) Comparison of background-corrected CV of anC:NP (blue), anC:NG (green) and anC (red) electrodes obtained at 20 mV s−1 in 0.015 M VO2+/1.5 M H_2SO_4.

peak-to-peak separation (ΔE_p) is >1.0 V. The introduction of N-functionalities leads to a reduction in both ΔE_p and the ratio between anodic and cathodic peak currents (J_{pa}/J_{pc}); however, the presence of pyrrolic-/pyridinic-N sites results in the most significant improvements: ΔE_p are 0.6 and 0.3 V for anC:N_G and anC:N_P, respectively, whereas J_{pa}/J_{pc} decreases from 3.4 to 1.3 when pyrrolic-/pyridinic-N sites are present. Capacitance corrected CV curves obtained at varying scan rates (10–50 mV s^{-1}) for anC:N_P (see **Fig. S4**) suggest good reversibility of the anC:N_P response over the scan rates tested, with peak currents varying as expected for a diffusion-controlled process at a disk electrode. This was confirmed by a log-log plot of anodic peak current (I_{pa}) vs scan rate which yielded a slope of 0.58 ± 0.01 [52,53] (**Fig. S4**). The above results indicate that nitrogen functional groups at the surface or within the carbon network improve charge transfer rates at the carbon electrodes and affect reversibility, while pyrrolic-/pyridinic-N sites appear to have a particularly beneficial effect. Notably, these effects arise from changes in the chemical make-up of the carbon material, rather than nanostructure or specific surface area [34,36,54–56], as all electrodes were prepared in the form of graphitized and topographically smooth films.

The VO^{2+}/VO_2^+ oxidation reaction was also evaluated via linear polarizations under rotation. Fig. 3**A** shows linear sweep voltammogram (LSV) curves obtained at 1600 rpm and 0.1 mV s^{-1} for anC, anC:N_G and anC:N_P. The potential at 10 μA cm^{-2} was found to shift anodically in the order anC:N_P < anC:N_G < anC (see Table 2), indicating that overpotentials for VO^{2+} oxidation at a given reaction rate are lower in the presence of pyrrolic-/pyridinic-N functionalities. LSVs were collected with an anodic limit of 1.3 V to avoid any inadvertent contributions from carbon corrosion [57,58]. This, however, prevented observation of mass transport-limited current plateaus (expected over 4.1–4.5 mA cm^{-2} based on published diffusion coefficients [37,59]) with the exception of anC:N_P which shows an inflection in the current density at the anodic potential limit. Tafel plots obtained from LSV data are shown in Fig. 3**B**. The Tafel plot for the nitrogen-free anC closely resembles that of graphite electrodes reported by Gattrell et al. [48] with visible shoulder and curvature at low overpotentials. Slope values were obtained over the potential ranges (indicated with thick lines in the figure) of 0.7–0.8 V, 0.85-0.95 V, and 1.0–1.1 V (vs Ag/AgCl) for anC:N_P, anC:N_G and anC, respectively, yielding values summarised in Table 2. In the case of anC:N_P the slope is close to 120 mV corresponding to a transfer coefficient α = 0.49; within Butler–Volmer's approximation this is consistent with the current density being limited by an electron transfer step. For the other two carbon materials the slopes are ca. 150 and 240 mV (α = 0.38 and 0.24 for anC:N_G and anC, respectively) which suggests that the reaction kinetics depart from that observed at anCN_P. The exchange current densities j_0 were estimated using the extrapolation method [60] and were found to decrease in the order anC:N_P > anC:N_G > anC (Table 2), as

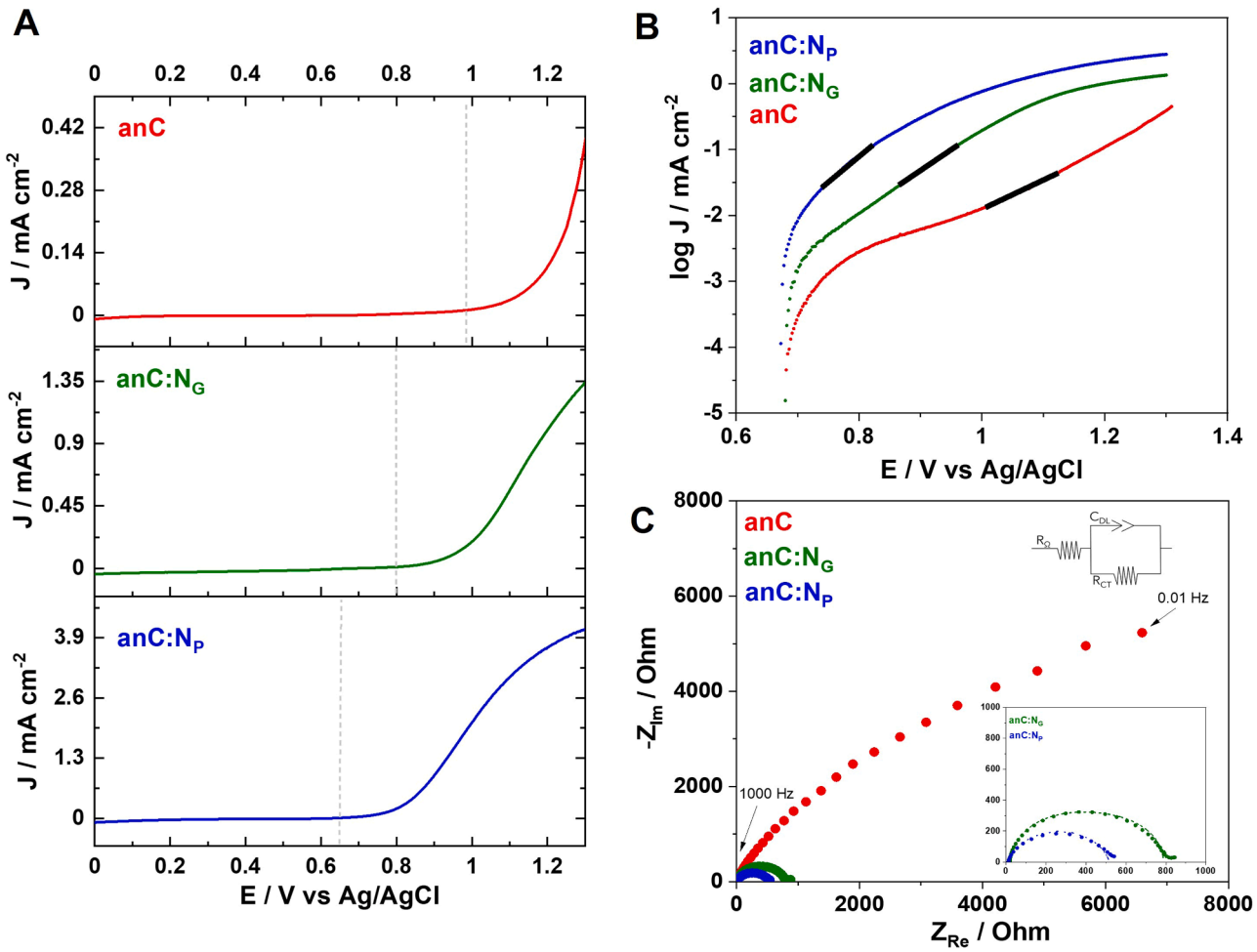

Fig. 3. LSV (A) and Tafel plots (B) obtained at 0.1 mV s^{-1} and 1600 rpm in 15 mM $VOSO_4$ in 1.5 M H_2SO_4. (C) Nyquist plots obtained from EIS studies at 0.88 V vs Ag/AgCl, at 1600 rpm over a frequency range 0.01–1000 Hz; the insets show an expanded view of the response from anC:N_G and anC:N_P and the equivalent circuit used to model the EIS response.

Table 2
Parameters obtained from LSV of VO^{2+} oxidation at 1600 rpm and 0.1 mV s^{-1} (Fig. 3): applied potential at 10 μA cm^{-2} (E), exchange current density (j_0) and charge transfer coefficient (α). Values reported are mean and standard deviation of three electrodes ($N = 3$).

Material	E@10 μA cm^{-2} (V vs Ag/AgCl)	j_0 (mA cm^{-2})	α	Tafel slope (mV)
anC	0.98	$(5.83 \pm 0.05) \times 10^{-4}$	0.24	241 ± 3
anC:N_G	0.79	$(2.09 \pm 0.04) \times 10^{-3}$	0.38	153 ± 2
anC:N_P	0.66	$(7.5 \pm 0.5) \times 10^{-3}$	0.49	118 ± 2

expected based on reversibility trends observed in the CV data. The j_0 of anC:N_P is an order of magnitude larger than that of N-free anC thus indicating a significant improvement resulting from the presence of N-sites.

EIS was also carried out to compare charge transfer rates across the three materials. Fig. 3**C** shows Nyquist plots obtained at 0.88 V vs Ag/AgCl at 1600 rpm over the frequency range 10^{-2}–10^{3} Hz. The plots are semi-circular, suggesting that the observed response is controlled by the kinetics of oxidation of VO^{2+} [7,40,61,62], and that the resistance to charge transfer is lowest for anC:N_P given its smallest intercept value on the real axis. Data was fitted using an equivalent circuit (see inset) which includes a constant phase element C_{DL} to represent the double layer, and resistances R_Ω and R_{ct} to represent the solution/cell and charge transfer resistances, respectively. Best-fit parameters thus obtained are summarized in Table 3. The R_{ct} in Fig. 3**C** were 787 and 507 Ω for anC:N_G and anC:N_P electrodes, respectively, while for anC the value is estimated to be >11,200 Ω. Both nitrogen-doped samples had similar charge transfer resistances that are more than an order of magnitude lower than that of nitrogen-free anC, thus supporting the positive effect of N-functionalities on the oxidation rate of vanadyl cations. The charge transfer resistance of an anC:N_P electrode was also evaluated at progressively increasing potentials yielding EIS results shown in **Fig. S5**. The R_{ct} decreases with increasing overpotential (**Table S3**) and a log plot of the inverse of the R_{ct} vs potential yielded a Tafel slope of 137 mV which is in reasonable agreement with the mean value obtained from LSV curves. The exchange current density was calculated via extrapolation using $j_0 = \frac{RT}{nFR_{ct}}$ [63,64], yielding $j_0 = 2.92 \times 10^{-2}$ mA cm^{-2}. This value is larger than that obtained via LSV, likely due to the conditions during EIS measurements more closely approaching the steady-state

Table 3
Comparison of parameters obtained from analysis of EIS at 0.88 V vs Ag/AgCl in 0.015 M $VO2^{+}$ and 1.5 M H_2SO_4 solutions. The equivalent circuit used is shown in Fig. 3C with the double layer capacitance simulated by impedance $Z_{CPE} = 1/T(i\omega)^p$.

Material	R_s (Ω)	R_{ct} (Ω)	T (F s^{p-1})	p
anC	9.2	>11,200	5.4×10^{-4}	0.80
anC:N_G	18	787	1.1×10^{-4}	0.93
anC:N_P	11	507	6.4×10^{-4}	0.84

[65].

Results obtained via voltammetry and EIS indicate that fast charge transfer and reversibility in the V(IV)/V(V) redox process correlate positively with the presence of pyridinic-/pyrrolic-N sites. To further discriminate the contributions of these functionalities, we fabricated anC electrodes modified with well-defined molecular adlayers of pyridyl groups using aryldiazonium cation reactions. Carbon substrates were functionalized via potential step reduction in aqueous solutions of diazotized 3-aminopyridine cations [49], as described in the experimental section and shown in Fig. 1**B**, obtaining electrodes referred to as anC-EPy. Fig. 4**A** shows XPS survey spectra of the anC substrate film compared to an anC film after functionalization (anC-EPy). Results show that after electrografting of pyridyl moieties a well-defined N 1s peak (400 eV) appears in the survey, in addition to the peaks arising from C 1s (285 eV) and O 1s (532 eV) emissions. The high-resolution spectrum of anC-EPy in the N1s region is shown in Fig. 4**B** and is in excellent agreement with that obtained by Agullo et al. [49] for organic films prepared in a similar manner on glassy carbon. The main component (399.3 eV, N_1) accounts for 65 % of the total signal and can be assigned to adsorbed pyridine molecular layers [66,67]; the binding energy suggests the presence of residual water which is further supported by an enhanced O 1s peak relative to anC, with binding energy consistent with that of H-donating water adlayers [67] (see **Fig. S6, Table S4**). A component at 400.5 eV (N_2) accounts for 26 % and suggests the presence of azo-group cross links, while the component at 401.9 eV (N_3) corresponds to protonated pyridinium groups [49,66,67]. XPS results therefore confirmed that molecular pyridyl adlayers are successfully formed on anC surfaces via the electrografting protocol used.

Fig. 4**C** shows corrected CV obtained at 0.020 V s^{-1} at anC-EPy in 0.015 M VO^{2+}/1.5 M H_2SO_4 compared to the response of the same material prior to functionalization with pyridyl moieties. The response is irreversible in the case of bare anC surfaces, as previously discussed, however, the pyridyl adlayer enhances both anodic and cathodic faradaic peaks associated with the VO^{2+}/VO_2^+ couple and the response displays improved reversibility. In the case of anC-EPy the ΔE_p was found to be 510 mV, while the J_{pa}/J_{pc} also increases to ca. 2.5 upon functionalization, which suggests improvements in reversibility even relative to anC:N_G materials. Fig. 4**D** shows also a comparison of the CV curves at 20 mV s^{-1} at anC-EPy and anC:N_P; the curves show that the molecular films lead to increased reversibility in all cases, but do not necessarily result in responses that are as reversible as those observed in the case of anC:N_P. This suggests that the presence of pyridinic groups might not be sufficient to completely explain the performance of anC:N_P. We propose that this is due to (i) pyrrolic-N groups being also important for improving the VO^{2+}/VO_2^+ electrochemical response, and/or (ii) faster response arising from pyridinic N-functionalities that are

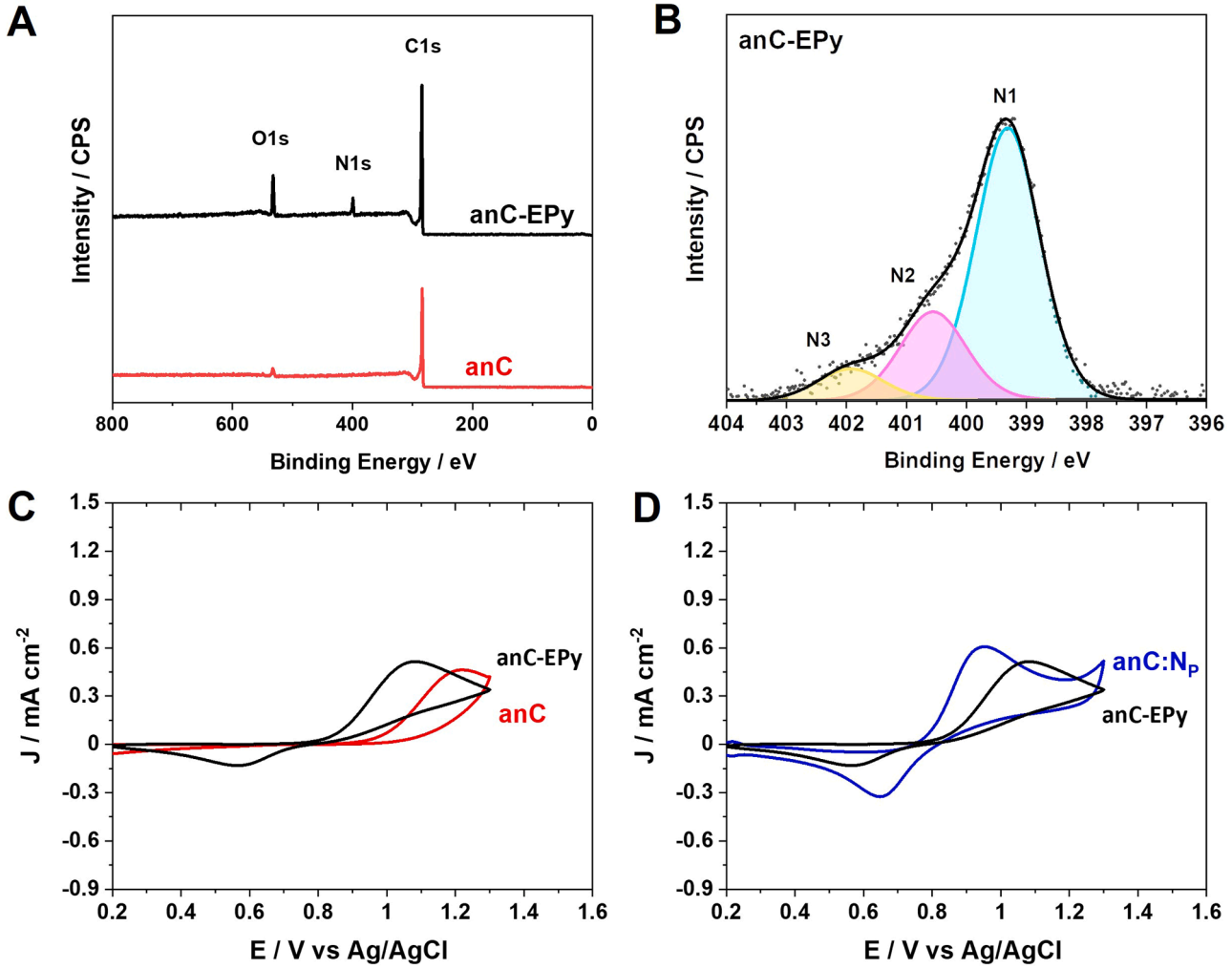

Fig. 4. (A) XPS survey spectra of anC carbon electrodes as deposited and after electrografting with aryldiazonium cations of 3-aminopyridine (anC-EPy). (B) High-resolution N 1s spectraum and best-fits of anC-EPy surfaces showing main components at 399.3, 400.5 and 401.9 eV. (C) Background-corrected CV at 0.020 V s^{-1} in 0.015 M VO^{2+}/1.5 M H_2SO_4 of: anC (red) vs anC-EPy (black); and (D) anC-EPy vs anC:Np.

embedded into the carbon scaffold in the form of condensed rings, rather than being wired to the nitrogen-free surface via C—C single bonds (as is the case after diazonium grafting).

3.2. Quantitative analysis of electrode kinetics using simulations

To compare our results to other reports in the literature, it is useful to obtain estimates of intrinsic rate constants that govern the reaction steps and to understand the impact of N-functionalities on the V(IV)/V(V) reaction mechanism. To this end we carried out simulations of the voltammograms obtained with the three different carbon electrodes using finite element methods. A range of mechanistic pathways have been proposed: Gattrell et al. [48] introduced early on a scheme of squares combining electrochemical (E) and chemical (C) steps (see **Fig. S7**), where the chemical steps consisted in protonation/deprotonation of aquo complexes. Possible schemes of greater complexity have also been discussed involving polynuclear complexes [68], sulfate/bisulfate adducts [48] and surface chemisorption [24]. However, the ECC mechanism has been previously found to be a satisfactory approach to modeling VO^{2+} oxidation, particularly at potentials away from the equilibrium value [37,48,69].

Following a strategy similar to that in [37], we first attempted the modeling of the anodic wave as a single E-step. Details of electrode geometry and boundary conditions are given in the Supplementary Information; briefly, a disk electrode geometry was assumed with vanadyl and pervanadyl concentrations of 15 and 0 mM, respectively, at time zero and at the bulk solution boundary. Diffusion coefficients $D_{VO^{2+}} = 2.1 \times 10^{-6}$ and $D_{VO_2^+} = 2.8 \times 10^{-6}$ $cm^2\,s^{-1}$ were taken from literature [59,70]; current densities were modeled according to Butler-Volmer kinetics and the transfer coefficient was assumed to be 0.5 [70]. Fig. 5**A** shows examples of a series of voltammograms generated by varying the heterogeneous rate constant k^0 in the range 10^{-8} – 10^{-3} $cm\,s^{-1}$. The experimental anodic waves of anC:Np, anC:Ng and anC can be compared to all 250 simulated anodic waves generated for different k^0, as shown in Fig. 5**B**. The best fit to the 1-electron E mechanism was obtained by locating the minimum of the sum of square errors (SSE) over a potential window preceding the peak potential. Fig. 5**C and D** shows best fit curves and errors, respectively, for the anodic waves of anC, anC:N_G and anC:N_P at 20 mV s^{-1} over the potential windows relevant to the fit. The simulated curves show good agreement with the experimental data yielding estimates of $k^0 = 1.29 \times 10^{-4}$, 9.25×10^{-6} and 9.34×10^{-7} $cm\,s^{-1}$ for anC:N_P, anC:N_G and anC, respectively.

Experimental k^0 values vary widely in the literature for carbon electrodes as a result of methodological differences and the extent to which reported results are corrected for electrode nanostructure and mass-transport effects, as highlighted by [32,36] and [37]. Nonetheless, we note that the k^0 thus estimated for anC is in good agreement with values reported for graphite [48,71] and GC [37] via methods that

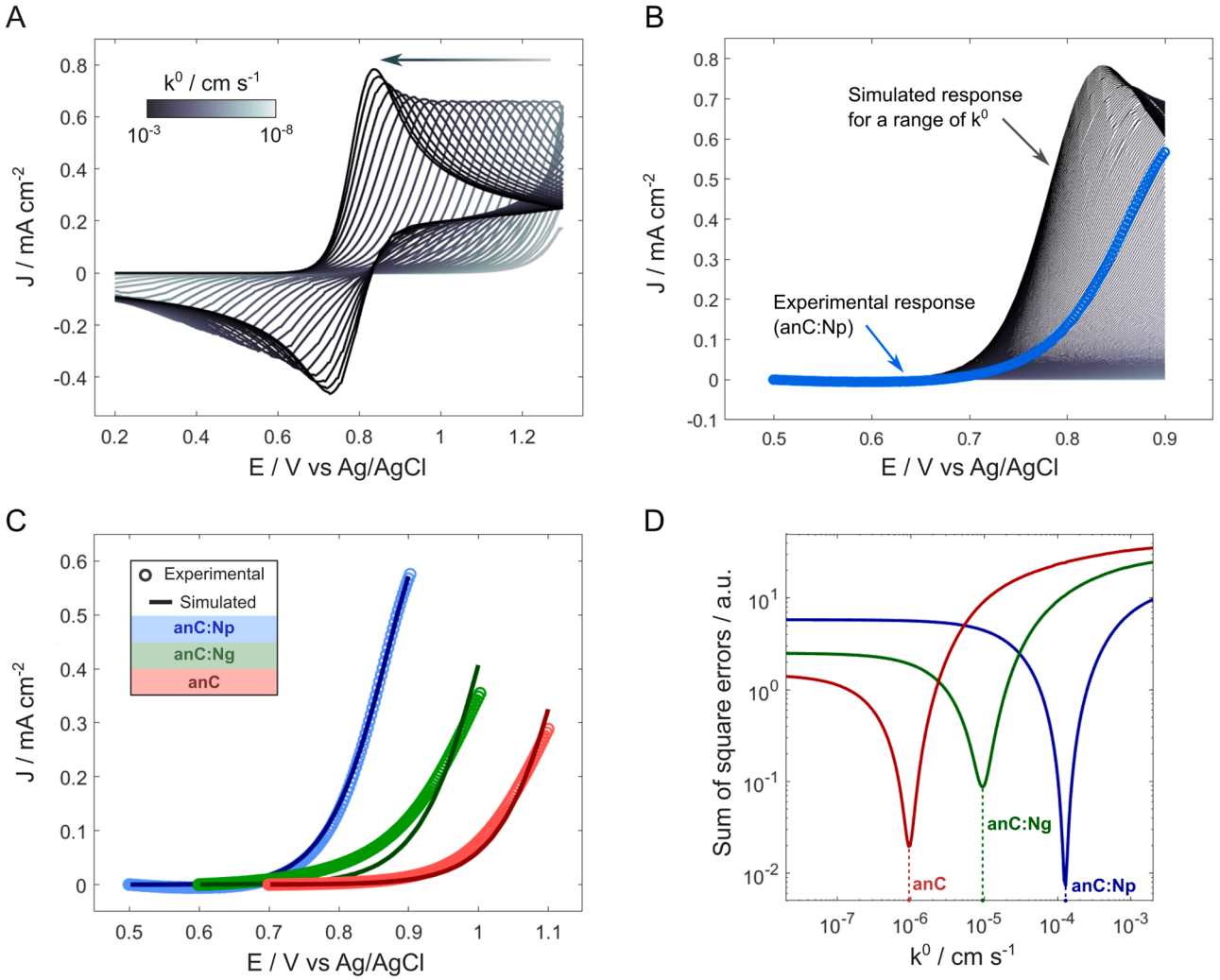

Fig. 5. (A) Examples of a series of CV curves simulated for an E-mechanism with k^0 ranging from 10^{-8} to 10^{-3} $cm\,s^{-1}$; only a sub-set of the simulated CV curves is shown for clarity of presentation. (B) Simulated voltammograms and experimental curve for anC:N_P (blue trace) in the anodic region of interest for best fits. (C) Best fit of the anodic waves of anC:N_P, anC:N_G and anC obtained from the minimum of (D) the sum of square errors as a function of k^0.

account for transport effects. The k^0 value of anC:N_P is ca. two orders of magnitude larger than at these nitrogen-free carbons thus indicating that the presence of basic nitrogenated moieties has a large impact on charge transfer rates for vanadyl oxidation. An expanded summary of k^0 estimates, including those obtained using porous/nanostructured electrodes is presented in **Table S8**.

A comparison of simulated vs experimental CV curves (see **Fig. S9**), however, indicates that it is not possible to model the CV using solely an E step because of strong discrepancies in position and magnitude of the reverse scan. Kaliyaraj and Compton [37] also observed a similar discrepancy when utilizing an E-mechanism to model $VO^{2+/}VO_2^+$ at GC surfaces. A more complex mechanism is thus required to reproduce the irreversible characteristics and peak breath of the cathodic waves. This was tackled via addition of a reversible chemical homogeneous step C characterised by forward and reverse rate constants k_{Cf} and k_{Cr}, respectively, to allow for an overall EC pathway (see **Fig. S8**). Fig. 6**A** shows examples of voltammograms simulated by using $k^0 = 1.29 \times 10^{-4}$ cm s^{-1} for anC:N_P and a series of k_{Cf} values in the range 10^{-3}–1 s^{-1} and k_{Cf}/k_{Cr} ratios in the range 0.05–50. The overlapping experimental voltammogram in the cathodic region is shown in Fig. 6**B**. It is evident that both the relative magnitude of k_{Cf} relative to k^0 and the thermodynamics of the C-step strongly affect the cathodic waveform. Best fits in Fig. 6**C** were obtained by identifying the minimum SSE as a function of both k_{Cf} and k_{Cf}/k_{Cr} ratios over the potential interval shown in the plots. A well-defined minimum was found over the ranges explored in all three cases, as shown in Fig. 6**D**. Best fit values obtained via this strategy are

Table 4
Kinetic rate constants obtained from simulations and best fits of CV curves using an EC mechanism. Uncertainties are defined by the range of values that results in a 10 % increase in the SSE relative to the best fit (see Supporting Information).

	k^0 (cm/s)	k_{Cf} (1/s)	k_{Cf}/k_{Cr}
anC:N_P	1.29×10^{-4}	10.3×10^{-2}	0.707
	(1.25; 1.30)	(8.30; 15.4)	(0.640; 0.812)
anC:N_G	9.25×10^{-6}	5.01×10^{-2}	2.14
	(8.71; 10.3)	(4.51; 7.28)	(1.93; 2.20)
anC	9.34×10^{-7}	4.87×10^{-2}	43.3
	(9.09; 9.97)	(4.72; 4.99)	(26.1; 105)

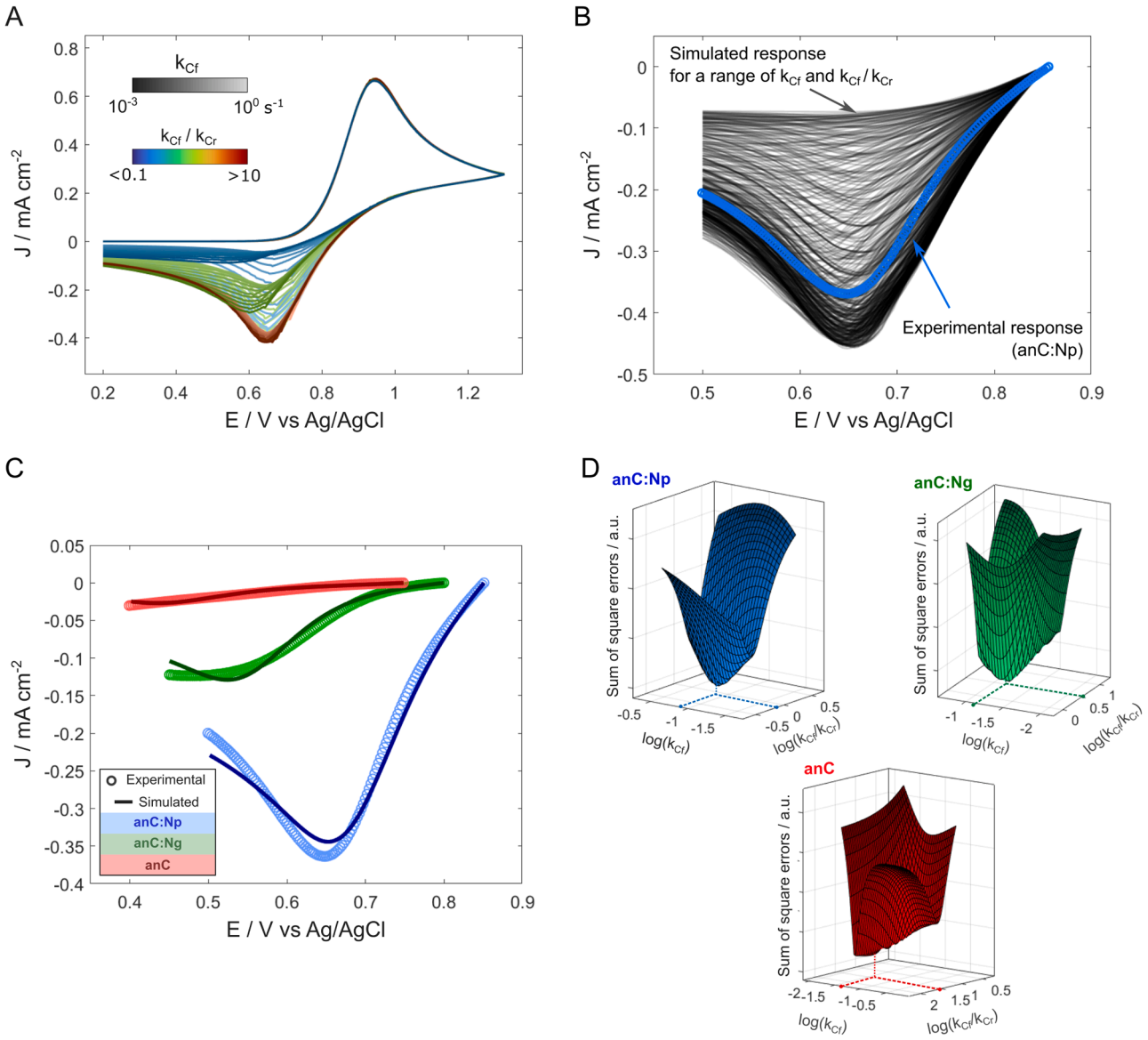

Fig. 6. (A) Examples of a series of CV curves simulated for an EC-mechanism with $k^0 = 1.29 \times 10^{-4}$ cm s^{-1} and a range of rate constants k_{Cf} and k_{Cr} as shown in the legend. (B) Simulated voltammograms and experimental curve for anC:N_P (blue trace) in the cathodic region of interest for best fits. (C) Best fits of the anodic waves of anC:N_P, anC:N_G and anC obtained from the minimum of (D) the sum of square errors as a function of k_{Cf} and of k_{Cf}/k_{Cr} ratios.

summarized in Table 4. It was found that best fits are obtained for k_{Cf} over the narrow range 0.05–0.10 s^{-1}, with values differing little across the three carbon materials studied. A comparison of simulated and experimental CV (see **Fig. S10**) also shows good agreement, indicating that an E rate limiting step followed by a C homogenous step better describes the overall reaction pathway for the VO^{2+}/VO_2^+ reaction. We note that these values were obtained under the assumption that a single standard potential for the vanadyl/pervanadyl couple is suitable for both anodic and cathodic waves, with no explicit dependence on pH included in the model [37].

4. Discussion

Overall, results from electrochemical studies on thin film carbon electrodes indicate that the presence of N-functionalities enhances rates of charge transfer for the VO^{2+}/VO_2^+ reaction. Importantly, a comparison of results for anC:N_G and anC:N_P, i.e. of two nitrogenated carbons with similar degrees of graphitization but differing distributions of N-functionalities, further indicates that basic N-sites, namely pyridinic-/pyrrolic-N, might play a beneficial role in improving charge transfer resistances and reversibility. This was further supported by the electrochemical response of nitrogen-free anC electrodes modified with pyridyl adlayers, which suggests that molecular pyridyl moieties at the electrolyte interface enhance the reversibility of the VO^{2+}/VO_2^+ response, albeit not to the extent observed at anC:N_P surfaces.

Results in Table 4 obtained via simulations of the voltametric waves under the assumption of an EC mechanism suggest that the presence of basic N-functionalities affects both electrochemical and chemical steps required to model the response of carbon materials. The heterogeneous rate constant of the electrochemical step increases significantly in the order anC < anC:N_G < anC:N_P with the greatest relative increase resulting from the introduction of basic N-functionalities at the carbon surface. This is in stark contrast with the effect of O-functionalities, which have been shown to negatively affect the intrinsic surface activity of carbon electrode materials in vanadyl/pervanadyl redox processes [32,34,36,72].

Interestingly, our results appear to support hypotheses put forward by others, suggesting that surface functionalities play a specific intrinsic role in improving charge transfer rates of the VO^{2+}/VO_2^+ couple [24,32,37]. It is reasonable to suggest that, given the satisfactory modeling of results with an EC mechanism, specific interactions between vanadium aquo complex/es and N-sites at carbon might be responsible for increased heterogeneous rate constants for the anodic reaction [73]. The ability of pyridyl groups to form complexes with V(IV) and V(V) centers is known in inorganic chemistry [74,75] and supported by recent computational work [31]; also, several N—O type ligands have been observed to alter oxidation rates and lower the (IV)/(V) half-wave potential in homogeneous reactions [75–77]. Hence, we speculate that related pyridyl-V interactions could play a role in modulating vanadyl oxidation at the carbon/eletrolyte interface, if sufficiently strong to displace protons in the acid electrolyte. Further support for this possibility might be gathered by observing that the difference in overpotential between materials in Table 2 are much greater than kT/e which is suggestive of surface-specific stabilization contributions [73].

Results in Table 4 also show that best fits yielded k_{Cf} values that are relatively independent of the carbon surface chemistry. On the other hand the k_{Cf}/k_{Cr} ratio, appears to strongly depend on the electrode material. The nature of the chemical equilibrium in C cannot be established on the basis of our model alone, however good candidates are deprotonation/protonation equilibria as in Fig. S8 [37,48]. The forward C step in this case, would be a deprotonation whose rate constant can be expected to be independent from electrode surface composition, in agreement with the narrow distribution of estimated k_{Cf} values. The reverse C step would be a pH-dependent protonation reaction (see Fig. S7), whose rate would be affected by local pH and, hence, by the presence of acid/base sites. The nitrogenated functionalities at carbon surfaces can modify the local pH and therefore could be expected to affect the effective/observed equilibrium constant k_{Cf}/k_{Cr} estimated from best fits. Despite chemical steps being modeled as homogeneous reactions and while not accounting explicitly for local chemical conditions, the model appears to capture general trends in the local environment experienced by the redox species resulting from changes in carbon surface composition. A more accurate model might consider contributions arising from both a homogeneous process (C_h) and a surface-dependent chemical reaction (C_s) leading to the overall C step. For carbon surfaces that do not display N-functionalities the homogeneous process would be expected to dominate the reaction pathway. The surface-dependent process might then play a major role only in the case of specific heteroatom functionalities at the electrolyte interface. This approach might indeed offer a more detailed (and accurate) physical description of the EC mechanism, however it would also increase the complexity of the simulations and best-fitting procedure for a correct deconvolution of C_h and C_s. This strategy would therefore benefit from further support, e.g. from experiments using local pH probes or via spectroscopic studies.

5. Conclusions

In this work we fabricated thin film carbon materials in the form of disk electrodes that are metal-free and that are either N-free or display predominantly graphitic-N or predominantly pyrrolic/pyridinic-N. We used these materials to study the electrochemical response of the V(IV)/V(V) redox couple as a function of chemical composition. Importantly, as the materials are deposited in the form of continuous thin solid films with identical thickness and all in intimate electrical contact with their glassy carbon disk supports, their response as a function of N-content and distribution can be studied without confounding effects arising from differences in mass transport or wettability as is often the case when studying other nanostructured carbos or drop-cast electrodes.

Our results obtained via voltammetry and EIS methods indicate that the presence of N-functionalities significantly enhances the intrinsic activity of carbon electrode surfaces. Both charge transfer rates and reversibility of the vanadyl oxidation reaction are improved, which are crucial for important applications such vanadium redox flow batteries. Voltammetry results could be modeled using an electrochemical-chemical (EC) mechanism via finite element simulations. Results indicate that the heterogeneous rate constant for the E-step can be increased by nearly two orders of magnitude relative to values observed at nitrogen-free electrodes by introducing basic pyrrolic-/pyridinic-N groups. We speculate that this is the result of specific stabilizing interactions at the carbon interface that are likely to modulate the resistance to charge transfer. Furthermore, results also suggest that N-functionalities might play a role in affecting the chemical step, possibly via local pH and/or protonation/deprotonation rates at the interface. However, further experimental work is needed to clarify the nature of these effects.

Notably, the effect of N-functionalities on the V(IV)/V(V) response is in contrast with the negative impact of O-groups demonstrated in recent work on vanadyl redox reactions [32,34,36,72]. This is likely due to the fact that N-functionalities, as opposed to O-groups, can be introduced into the carbon scaffold without necessarily increasing the insulating character of carbons/nanocarbons. In fact, they can improve metallic character and density of states at the Fermi level if judiciously incorporated into the matrix [29,78,79], thus offering an interesting route to the effective design of advanced carbon electrodes with high conductivity and chemical active sites for VRFB devices.

CRediT authorship contribution statement

Maida A. Costa de Oliveira: Conceptualization, Methodology, Validation, Formal analysis, Investigation, Data curation, Project administration, Funding acquisition. **Christian Schröder:** Formal

analysis, Investigation, Data curation, Writing – original draft. **Marc Brunet Cabré:** Methodology, Software, Formal analysis, Investigation, Data curation, Writing – original draft. **Hugo Nolan:** Investigation. **Antoni Forner-Cuenca:** Conceptualization. **Tatiana S. Perova:** Investigation, Resources. **Kim McKelvey:** Methodology, Formal analysis, Resources. **Paula E. Colavita:** Conceptualization, Methodology, Validation, Formal analysis, Resources, Data curation, Supervision, Project administration, Funding acquisition, Writing – original draft.

Declaration of Competing Interest

The authors declare the following financial interests/personal relationships which may be considered as potential competing interests: Kim McKelvey reports equipment, drugs, or supplies was provided by Park Systems Corp.

Data availability

Data will be made available on request.

Acknowledgements

The research conducted in this publication was funded by the Irish Research Council under grant number GOIPD/2021/530 and also by Science Foundation Ireland under Grant No. 19/FFP/6761. This project also received support from the European Union's Horizon 2020 research and innovation program under the Marie Skłodowska-Curie Grant Agreement No. 713567 (EDGE-Project HECAT4H2). The results of this publication reflect only the authors' view and the Commission is not responsible for any use that may be made of the information it contains. We gratefully acknowledge support from Park Systems for their loan of a Park NX10 instrument. Use of the XPS of I. V. Shvets and C. McGuinness provided under SFI Equipment Infrastructure funds.

Supplementary materials

Supplementary material associated with this article can be found, in the online version, at doi:10.1016/j.electacta.2023.143640.

References

[1] M. Skyllas-Kazacos, Review—highlights of UNSW all-vanadium redox battery development: 1983 to present, J. Electrochem. Soc. 169 (2022), 070513.
[2] M. Skyllas-Kazacos, M. Rychcik, R.G. Robins, A.G. Fane, M.A. Green, New all-vanadium redox flow cell, J. Electrochem. Soc. 133 (1986) 1057.
[3] M. Skyllas-Kazacos, C. Menictas, Vanadium redox flow batteries, in: L.F. Cabeza (Ed.), Encyclopedia of Energy Storage, Elsevier, Oxford, 2022, pp. 407–422.
[4] J. Kim, H. Park, Experimental analysis of discharge characteristics in vanadium redox flow battery, Appl. Energy 206 (2017) 451–457.
[5] L. Wu, J. Wang, Y. Shen, L. Liu, J. Xi, Electrochemical evaluation methods of vanadium flow battery electrodes, Phys. Chem. Chem. Phys. 19 (2017) 14708–14717.
[6] Y. Li, S. Yang, Y. Zhao, N. Mubarak, M. Xu, M. Ihsan-Ul-Haq, T. Zhao, Q. Chen, J.-K. Kim, Deciphering the exceptional kinetics of hierarchical nitrogen-doped carbon electrodes for high-performance vanadium redox flow batteries, J. Mater. Chem. A 10 (2022) 5605–5613.
[7] W. Wang, X. Fan, Y. Qin, J. Liu, C. Yan, C. Zeng, The reduction reaction kinetics of vanadium(V) in acidic solutions on a platinum electrode with unusual difference compared to carbon electrodes, Electrochim. Acta 283 (2018) 1313–1322.
[8] M. Skyllas-Kazacos, F. Grossmith, Efficient vanadium redox flow cell, J. Electrochem. Soc. 134 (1987) 2950.
[9] D. Dixon, D.J. Babu, A. Bhaskar, H.-M. Bruns, J.J. Schneider, F. Scheiba, H. Ehrenberg, Tuning the performance of vanadium redox flow batteries by modifying the structural defects of the carbon felt electrode, Beilstein J. Nanotechnol. 10 (2019) 1698–1706.
[10] M.-A. Goulet, M. Skyllas-Kazacos, E. Kjeang, The importance of wetting in carbon paper electrodes for vanadium redox reactions, Carbon N.Y. 101 (2016) 390–398.
[11] B. Sun, M. Skyllas-Kazacos, Modification of graphite electrode materials for vanadium redox flow battery application—I. Thermal treatment, Electrochim. Acta 37 (1992) 1253–1260.
[12] M. Becker, N. Bredemeyer, N. Tenhumberg, T. Turek, Kinetic studies at carbon felt electrodes for vanadium redox-flow batteries under controlled transfer current density conditions, Electrochim. Acta 252 (2017) 12–24.
[13] A. Forner-Cuenca, F.R. Brushett, Engineering porous electrodes for next-generation redox flow batteries: recent progress and opportunities, Curr. Opin. Electrochem. 18 (2019) 113–122.
[14] W. Wang, Z. Wei, W. Su, X. Fan, J. Liu, C. Yan, C. Zeng, Kinetic investigation of vanadium (V)/(IV) redox couple on electrochemically oxidized graphite electrodes, Electrochim. Acta 205 (2016) 102–112.
[15] K.V. Greco, A. Forner-Cuenca, A. Mularczyk, J. Eller, F.R. Brushett, Elucidating the nuanced effects of thermal pretreatment on carbon paper electrodes for vanadium redox flow batteries, ACS Appl. Mater. Interfaces 10 (2018) 44430–44442.
[16] M.Z. Jelyani, S. Rashid-Nadimi, S. Asghari, Treated carbon felt as electrode material in vanadium redox flow batteries: a study of the use of carbon nanotubes as electrocatalyst, J. Solid State Electrochem. 21 (2017) 69–79.
[17] W. Li, J. Liu, C. Yan, Reduced graphene oxide with tunable C/O ratio and its activity towards vanadium redox pairs for an all vanadium redox flow battery, Carbon N.Y. 55 (2013) 313–320.
[18] A. Xu, L. Shi, L. Zeng, T.S. Zhao, First-principle investigations of nitrogen-, boron-, phosphorus-doped graphite electrodes for vanadium redox flow batteries, Electrochim. Acta 300 (2019) 389–395.
[19] M. Meskinfam Langroudi, C.S. Pomelli, R. Giglioli, C. Chiappe, M. Aysla Costa de Oliveira, B. Mecheri, S. Licoccia, A. D'Epifanio, Interaction of vanadium species with a functionalized graphite electrode: a combined theoretical and experimental study for flow battery applications, J. Power Sources 420 (2019) 134–142.
[20] H.R. Jiang, W. Shyy, L. Zeng, R.H. Zhang, T.S. Zhao, Highly efficient and ultra-stable boron-doped graphite felt electrodes for vanadium redox flow batteries, J. Mater. Chem. A 6 (2018) 13244–13253.
[21] Q. Li, J. Wang, T. Zhang, Z. Wang, Z. Xue, J. Li, H. Sun, Analysis of the performance of phosphorus and sulphur co-doped reduced graphene oxide as catalyst in vanadium redox flow battery, J. Electrochem. Soc. 169 (2022), 010523.
[22] Y. Shao, X. Wang, M. Engelhard, C. Wang, S. Dai, J. Liu, Z. Yang, Y. Lin, Nitrogen-doped mesoporous carbon for energy storage in vanadium redox flow batteries, J. Power Sources 195 (2010) 4375–4379.
[23] T. Wu, K. Huang, S. Liu, S. Zhuang, D. Fang, S. Li, D. Lu, A. Su, Hydrothermal ammoniated treatment of PAN-graphite felt for vanadium redox flow battery, J. Solid State Electrochem. 16 (2012) 579–585.
[24] M.-y. Liu, Z.-p. Xiang, J.-h. Piao, J.-y. Shi, Z.-x. Liang, Electrochemistry of vanadium redox couples on nitrogen-doped carbon, Electrochim. Acta 259 (2018) 687–693.
[25] K. Zhang, C. Yan, A. Tang, Interfacial co-polymerization derived nitrogen-doped carbon enables high-performance carbon felt for vanadium flow batteries, J. Mater. Chem. A 9 (2021) 17300–17310.
[26] Q. Ma, X.-X. Zeng, C. Zhou, Q. Deng, P.-F. Wang, T.-T. Zuo, X.-D. Zhang, Y.-X. Yin, X. Wu, L.-Y. Chai, Y.-G. Guo, Designing high-performance composite electrodes for vanadium redox flow batteries: experimental and computational investigation, ACS Appl. Mater. Interfaces 10 (2018) 22381–22388.
[27] L. Shi, S. Liu, Z. He, J. Shen, Nitrogen-Doped Graphene:effects of nitrogen species on the properties of the vanadium redox flow battery, Electrochim. Acta 138 (2014) 93–100.
[28] M.K. Hoque, J.A. Behan, S.N. Stamatin, F. Zen, T.S. Perova, P.E. Colavita, Capacitive storage at nitrogen doped amorphous carbon electrodes: structural and chemical effects of nitrogen incorporation, RSC Adv. 9 (2019) 4063–4071.
[29] J.A. Behan, S.N. Stamatin, M.K. Hoque, G. Ciapetti, F. Zen, L. Esteban-Tejeda, P. E. Colavita, Combined optoelectronic and electrochemical study of nitrogenated carbon electrodes, J. Phys. Chem. C 121 (2017) 6596–6604.
[30] J. Etula, N. Wester, T. Liljeström, S. Sainio, T. Palomäki, K. Arstila, T. Sajavaara, J. Koskinen, M.A. Caro, T. Laurila, What determines the electrochemical properties of nitrogenated amorphous carbon thin films? Chem. Mater. 33 (2021) 6813–6824.
[31] C.T.-C. Wan, D. López Barreiro, A. Forner-Cuenca, J.-W. Barotta, M.J. Hawker, G. Han, H.-C. Loh, A. Masic, D.L. Kaplan, Y.-M. Chiang, F.R. Brushett, F.J. Martin-Martinez, M.J. Buehler, Exploration of biomass-derived activated carbons for use in vanadium redox flow batteries, ACS Sustain. Chem. Eng. 8 (2020) 9472–9482.
[32] H. Fink, J. Friedl, U. Stimming, Composition of the electrode determines which half-cell's rate constant is higher in a vanadium flow battery, J. Phys. Chem. C 120 (2016) 15893–15901.
[33] X.W. Wu, T. Yamamura, S. Ohta, Q.X. Zhang, F.C. Lv, C.M. Liu, K. Shirasaki, I. Satoh, T. Shikama, D. Lu, S.Q. Liu, Acceleration of the redox kinetics of VO^{2+}/VO_2^+ and V^{3+}/V^{2+} couples on carbon paper, J. Appl. Electrochem. 41 (2011) 1183–1190.
[34] J. Friedl, C.M. Bauer, A. Rinaldi, U. Stimming, Electron transfer kinetics of the VO^{2+}/VO_2^+ – Reaction on multi-walled carbon nanotubes, Carbon N.Y. 63 (2013) 228–239.
[35] H. Radinger, A. Ghamlouche, H. Ehrenberg, F. Scheiba, Origin of the catalytic activity at graphite electrodes in vanadium flow batteries, J. Mater. Chem. A 9 (2021) 18280–18293.
[36] J. Friedl, U. Stimming, Determining electron transfer kinetics at porous electrodes, Electrochim. Acta 227 (2017) 235–245.
[37] A. Kaliyaraj Selva Kumar, R.G. Compton, Single-Entity "Nano-catalysis": carbon nanotubes and the VO^{2+}/VO_2^+ redox reaction, ACS Catal. 12 (2022) 4754–4764.
[38] T. Tichter, J. Schneider, C. Roth, Finite heterogeneous rate constants for the electrochemical oxidation of VO^{2+} at glassy carbon electrodes, Front. Energy Res. 8 (2020) 155.
[39] T. Tichter, D. Andrae, J. Mayer, J. Schneider, M. Gebhard, C. Roth, Theory of cyclic voltammetry in random arrays of cylindrical microelectrodes applied to carbon felt

electrodes for vanadium redox flow batteries, Phys. Chem. Chem. Phys. 21 (2019) 9061–9068.
[40] I. Kroner, M. Becker, T. Turek, Determination of rate constants and reaction orders of vanadium-ion kinetics on carbon fiber electrodes, ChemElectroChem 7 (2020) 4314–4325.
[41] M.-A. Goulet, M. Eikerling, E. Kjeang, Direct measurement of electrochemical reaction kinetics in flow-through porous electrodes, Electrochem. Commun. 57 (2015) 14–17.
[42] H. Nolan, C. Schröder, M. Brunet-Cabré, F. Pota, N. McEvoy, K. McKelvey, T. S. Perova, P.E. Colavita, MoS2/carbon heterostructured catalysts for the hydrogen evolution reaction: n-doping modulation of substrate effects in acid and alkaline electrolytes, Carbon N.Y. 202 (2023) 70–80.
[43] J.A. Behan, E. Mates-Torres, S.N. Stamatin, C. Domínguez, A. Iannaci, K. Fleischer, M.K. Hoque, T.S. Perova, M. García-Melchor, P.E. Colavita, Untangling cooperative effects of pyridinic and graphitic nitrogen sites at metal-free N-doped carbon electrocatalysts for the oxygen reduction reaction, Small 15 (2019), 1902081.
[44] J.A. Behan, A. Iannaci, C. Domìnguez, S.N. Stamatin, M.K. Hoque, J. M. Vasconcelos, T. Perova, P.E. Colavita, Electrocatalysis of N-doped Carbons in the Oxygen Reduction Reaction as a function of pH: n-sites and Scaffold Effects, Carbon N.Y. 148 (2019) 224–230.
[45] C. Domìnguez, J.A. Behan, P.E. Colavita, Electrocatalysis at nanocarbons: model systems and applications in energy conversion, in: N. Yang, G. Zhao, J.S. Foord (Eds.), Nanocarbon Electrochemistry, John Wiley & Sons, Ltd, Chichester, 2020, pp. 201–250.
[46] M. Favaro, L. Perini, S. Agnoli, C. Durante, G. Granozzi, A. Gennaro, Electrochemical behavior of N and Ar implanted highly oriented pyrolytic graphite substrates and activity toward oxygen reduction reaction, Electrochim. Acta 88 (2013) 477–487.
[47] D. Guo, R. Shibuya, C. Akiba, S. Saji, T. Kondo, J. Nakamura, Active sites of nitrogen-doped carbon materials for oxygen reduction reaction clarified using model catalysts, Science 351 (2016) 361–365.
[48] M. Gattrell, J. Park, B. Macdougall, J. Apte, S. McCarthy, C.W. Wu, Study of the mechanism of the vanadium 4+/5+ redox reaction in acidic solutions, J. Electrochem. Soc. 151 (2004) A123.
[49] J. Agullo, M. Morin, D. Bélanger, Modification of glassy carbon electrode by electrografting of in situ generated 3-diazopyridinium cations, J. Electrochem. Soc. 159 (2012) H758–H764.
[50] R. Guidelli, R.G. Compton, J.M. Feliu, E. Gileadi, J. Lipkowski, W. Schmickler, S. Trasatti, Defining the transfer coefficient in electrochemistry: an assessment (IUPAC Technical Report), Pure Appl. Chem. 86 (2014) 245–258.
[51] W.M. Haynes, CRC handbook of chemistry and physics, 97th ed., CRC press2016.
[52] J.A. Behan, F. Grajkowski, D.R. Jayasundara, L. Vilella-Arribas, M. García-Melchor, P.E. Colavita, Influence of carbon nanostructure and oxygen moieties on dopamine adsorption and charge transfer kinetics at glassy carbon surfaces, Electrochim. Acta 304 (2019) 221–230.
[53] J.A. Behan, M.K. Hoque, S.N. Stamatin, T.S. Perova, L. Vilella-Arribas, M. García-Melchor, P.E. Colavita, Experimental and computational study of dopamine as an electrochemical probe of the surface nanostructure of graphitized N-doped carbon, J. Phys. Chem. C 122 (2018) 20763–20773.
[54] E.J.F. Dickinson, I. Streeter, R.G. Compton, Theory of Chronoamperometry at cylindrical microelectrodes and their arrays, J. Phys. Chem. C 112 (2008) 11637–11644.
[55] M.C. Henstridge, E.J.F. Dickinson, M. Aslanoglu, C. Batchelor-McAuley, R. G. Compton, Voltammetric selectivity conferred by the modification of electrodes using conductive porous layers or films: the oxidation of dopamine on glassy carbon electrodes modified with multiwalled carbon nanotubes, Sens. Actuators B 145 (2010) 417–427.
[56] C. Punckt, M.A. Pope, I.A. Aksay, On the electrochemical response of porous functionalized graphene electrodes, J. Phys. Chem. C 117 (2013) 16076–16086.
[57] S.J. Ashton, M. Arenz, A DEMS study on the electrochemical oxidation of a high surface area carbon black, Electrochem. Commun. 13 (2011) 1473–1475.
[58] S.G. Ji, H. Kim, W.H. Lee, H.-S. Oh, C.H. Choi, Real-time monitoring of electrochemical carbon corrosion in alkaline media, J. Mater. Chem. A 9 (2021) 19834–19839.
[59] S. Zhong, M. Skyllas-Kazacos, Electrochemical behaviour of vanadium(V)/ vanadium(IV) redox couple at graphite electrodes, J. Power Sources 39 (1992) 1–9.
[60] J. Tafel, Über die Polarisation bei kathodischer Wasserstoffentwicklung, Z. Phys. Chem. (1905) 641–712 (Muenchen, Ger.), 50U.
[61] P. Leuaa, D. Priyadarshani, D. Choudhury, R. Maurya, M. Neergat, Resolving charge-transfer and mass-transfer processes of VO^{2+}/VO_2^+ redox species across the electrode/electrolyte interface using electrochemical impedance spectroscopy for vanadium redox flow battery, RSC Adv. 10 (2020) 30887–30895.
[62] M. Jing, C. Li, X. An, Z. Xu, J. Liu, C. Yan, D. Fang, X. Fan, Systematic investigation of the physical and electrochemical characteristics of the vanadium (III) acidic electrolyte with different concentrations and related diffusion kinetics, Front. Chem. 8 (2020) 502.
[63] D.O. Opar, R. Nankya, J. Lee, H. Jung, Assessment of three-dimensional nitrogen-doped mesoporous graphene functionalized carbon felt electrodes for high-performance all vanadium redox flow batteries, Appl. Surf. Sci. 531 (2020), 147391.
[64] C. Choi, H. Noh, S. Kim, R. Kim, J. Lee, J. Heo, H.-T. Kim, Understanding the redox reaction mechanism of vanadium electrolytes in all-vanadium redox flow batteries, J. Energy Storage 21 (2019) 321–327.
[65] D. Li, C. Lin, C. Batchelor-McAuley, L. Chen, R.G. Compton, Tafel analysis in practice, J. Electroanal. Chem. 826 (2018) 117–124.
[66] A. Boucly, F. Rochet, Q. Arnoux, J.J. Gallet, F. Bournel, H. Tissot, V. Marry, E. Dubois, L. Michot, Soft x-ray heterogeneous radiolysis of pyridine in the presence of hydrated strontium-hydroxyhectorite and its monitoring by near-ambient pressure photoelectron spectroscopy, Sci. Rep. 8 (2018) 6164.
[67] Y. Zubavichus, M. Zharnikov, Y. Yang, O. Fuchs, E. Umbach, C. Heske, A. Ulman, M. Grunze, X-ray photoelectron spectroscopy and near-edge x-ray absorption fine structure study of water adsorption on pyridine-terminated thiolate self-assembled monolayers, Langmuir 20 (2004) 11022–11029.
[68] W. Wang, X. Fan, J. Liu, C. Yan, C. Zeng, A novel mechanism for the oxidation reaction of $VO2^+$ on a graphite electrode in acidic solutions, J. Power Sources 261 (2014) 212–220.
[69] J.S. Lawton, S.M. Tiano, D.J. Donnelly, S.P. Flanagan, T.M. Arruda, The effect of sulfuric acid concentration on the physical and electrochemical properties of vanadyl solutions, Batteries 4 (2018) 40.
[70] T. Yamamura, N. Watanabe, T. Yano, Y. Shiokawa, Electron-transfer kinetics of Np^{3+}/ Np^{4+}, NpO^{2+}/ NpO_2^{2+}, V^{2+}/ V^{3+}, and VO^{2+}/ VO_2^+ at carbon electrodes, J. Electrochem. Soc. 152 (2005) A830.
[71] Y. Wen, H. Zhang, P. Qian, P. Zhao, H. Zhou, B. Yi, Investigations on the electrode process of concentrated V(IV)/V(V) species in a vanadium redox flow battery, Acta Phys. Chim. Sin. 22 (2006) 403–408.
[72] R.M. Bachman, D.M. Hall, L.R. Radovic, On the electrocatalytically active sites in graphene-based vanadium redox flow batteries, Carbon N.Y. 201 (2023) 891–899.
[73] S. Fletcher, Tafel slopes from first principles, J. Solid State Electrochem. 13 (2009) 537–549.
[74] D.C. Crans, A.S. Tracey, The chemistry of vanadium in aqueous and nonaqueous solution. Vanadium Compounds, American Chemical Society, Washington DC, 1998, pp. 2–29.
[75] P. Galloni, V. Conte, B. Floris, A journey into the electrochemistry of vanadium compounds, Coord. Chem. Rev. 301–302 (2015) 240–299.
[76] K. Saito, Y. Sasaki, Characteristics of electron transfer reactions of early transition elements, Pure Appl. Chem. 60 (1988) 1123–1132.
[77] M. Nishizawa, Y. Sasaki, K. Saito, Kinetics and mechanisms of the outer-sphere oxidation of cis-aquaoxovanadium(IV) complexes containing quadrindentate amino polycarboxylates. Interpretation of the difference in activation parameters with the charge type of reactants, Inorg. Chem. 24 (1985) 767–772.
[78] T. Schiros, D. Nordlund, L. Pálová, D. Prezzi, L. Zhao, K.S. Kim, U. Wurstbauer, C. Gutiérrez, D. Delongchamp, C. Jaye, D. Fischer, H. Ogasawara, L.G. M. Pettersson, D.R. Reichman, P. Kim, M.S. Hybertsen, A.N. Pasupathy, Connecting dopant bond type with electronic structure in N-doped graphene, Nano Lett. 12 (2012) 4025–4031.
[79] C. Ma, Q. Liao, H. Sun, S. Lei, Y. Zheng, R. Yin, A. Zhao, Q. Li, B. Wang, Tuning the doping types in graphene sheets by N monoelement, Nano Lett. 18 (2018) 386–394.